

DYNAMIC AND CONVECTIVE RESULTS FOR A DEVELOPING LAMINAR UNSTEADY FLOW

R. CREFF AND P. ANDRE

Laboratoire de Mécanique et d'énergie—ESEM, Université d'Orléans, 45046 Orléans Cedex, France

AND

J. BATINA

Laboratoire d'Analyse Numérique—U.E.R. S.F.A., Université d'Orléans, 45046 Orléans Cedex, France

SUMMARY

Dynamic and thermal results for developing laminar pulsed flows in a duct are presented. They have been investigated by means of a finite difference model. This flow is described in terms of an unsteady pulsed flow superimposed on a steady incompressible one with the following main assumptions: a sinusoidal modulation for the pulsation and a uniform wall temperature. Results emphasize the importance of this entry region, where four simultaneous developments occur: steady—dynamic and thermal—and unsteady—dynamic and thermal.

INTRODUCTION

Some results for a developing laminar pulsed flow in a duct, undertaken by means of a finite-difference method, are presented. This model is specifically built to treat this particular convective problem where the flow is described in terms of an unsteady pulsed flow, superimposed on a steady incompressible one. Consequently four developing zones: steady dynamic and thermal and unsteady dynamic and thermal occur beyond the duct entry. The main hypotheses retained are an unsteady flow generated by a sinusoidal axial pressure gradient, and a uniform wall temperature.

This specific model is supposed to give a better understanding of the complicated process of unsteady heat transfer, occurring in this developing zone. Most of the previous works have been done under the simplified assumption of a fully developed—dynamic and thermal—steady flow.^{1,2} The proposed model³ is particularly suitable to treat this important convective problem of developing flows.

EQUATIONS AND BOUNDARY CONDITIONS

The physical problem and its boundary conditions are given in Figure 1.

$$\text{For } x = 0: \left. \begin{array}{l} u = U \\ v = 0 \\ T = T_{\infty} \end{array} \right\} \forall r, \forall t.$$

$$\text{For } t = 0; \quad \frac{\partial u}{\partial r} = \frac{\partial T}{\partial r} = v = 0, \quad \forall x, \forall t.$$

$$\text{For } r = R; \quad u = v = 0 \quad \text{and} \quad T = T_w = \text{constant} \quad \forall x, \forall t.$$

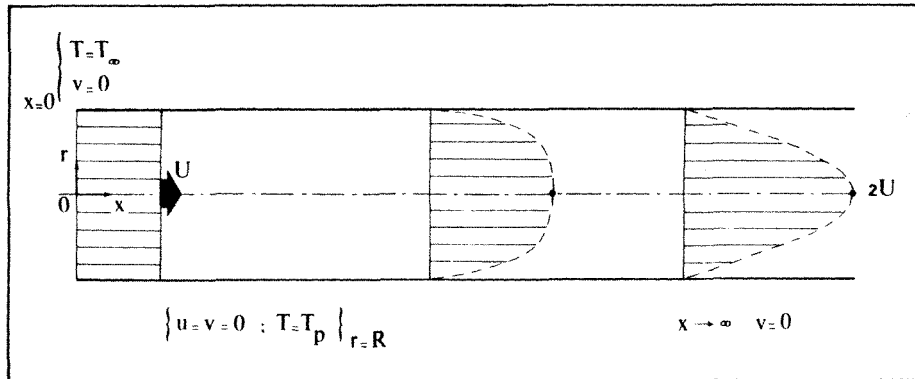


Figure 1. Boundary conditions

From these boundary conditions, the equation system can be written as follows:

$$\frac{\partial u}{\partial x} + \frac{1}{r} \frac{\partial}{\partial r}(rv) = 0, \quad (1)$$

$$\frac{\partial u}{\partial t} + \frac{1}{r} \frac{\partial}{\partial r}(rvu) + \frac{\partial}{\partial x}(u^2) = -\frac{1}{\rho} \frac{\partial p}{\partial x} + \frac{\mu}{\rho} \left[\frac{\partial^2 u}{\partial r^2} + \frac{1}{r} \frac{\partial u}{\partial r} \right], \quad (2)$$

$$\frac{\partial v}{\partial t} + \frac{1}{r} \frac{\partial}{\partial r}(rv^2) + \frac{\partial}{\partial x}(uv) = -\frac{1}{\rho} \frac{\partial p}{\partial r} + \frac{\mu}{\rho} \left[\frac{\partial^2 v}{\partial r^2} + \frac{1}{r} \frac{\partial v}{\partial r} - \frac{v}{r^2} \right], \quad (3)$$

$$\frac{\partial T}{\partial t} + \frac{1}{r} \frac{\partial}{\partial r}(rvT) + \frac{\partial}{\partial x}(uT) = \frac{k}{\rho C_p} \left[\frac{\partial^2 T}{\partial r^2} + \frac{1}{r} \frac{\partial T}{\partial r} \right]. \quad (4)$$

Owing to the size of the Péclet number used in the following developments, it can be assumed that the axial conduction term $\partial^2 T / \partial x^2$ is negligible compared to the radial conduction.

To solve the equations system, each quantity: u , v , p , T is seen in terms of an asymptotic development in a complex form such as

$$f(x_1 \cdots x_p) = \sum_{n=0}^{\infty} a_n f_n(\varepsilon, x_1 \cdots x_p); \quad n \in N,$$

with ε a small parameter less than unity, called the perturbation parameter, and a_n a series of complex or real coefficients.

Assuming that the axial pressure gradient p'_x is given by

$$p'_x = \text{Re}[p'_{x0} + \varepsilon^1 p'_{x1} e^{j\omega t}]$$

then, as an example, the axial velocity can be written as follows:

$$u = u_0 + \varepsilon^1 u_1 e^{j\omega t} + \varepsilon^2 u_2 e^{2j\omega t} + \dots$$

The equations are then identified to the ε^0 and ε^1 orders.

For the zeroth order:

$$\frac{\partial u_0}{\partial x} + \frac{1}{r} \frac{\partial}{\partial r}(rv_0) = 0, \quad (5)$$

$$\frac{1}{r} \frac{\partial}{\partial r} (r u_0 v_0) + \frac{\partial}{\partial x} (u_0^2) = -\frac{1}{\rho} p'_{x0} + \nu \left[\frac{\partial^2 u_0}{\partial r^2} + \frac{1}{r} \frac{\partial u_0}{\partial r} \right], \quad (6)$$

$$\frac{1}{r} \frac{\partial}{\partial r} (r v_0^2) + \frac{\partial}{\partial x} (u_0 v_0) = -\frac{1}{\rho} p'_{r0} + \nu \left[\frac{\partial^2 v_0}{\partial r^2} + \frac{1}{r} \frac{\partial v_0}{\partial r} - \frac{v_0}{r^2} \right], \quad (7)$$

$$\frac{1}{r} \frac{\partial}{\partial r} (r v_0 T_0) + \frac{\partial}{\partial x} (u_0 T_0) = \frac{k}{\rho C_p} \left[\frac{\partial^2 T_0}{\partial r^2} + \frac{1}{r} \frac{\partial T_0}{\partial r} \right]. \quad (8)$$

For the first order:

$$\frac{\partial u_1}{\partial x} + \frac{1}{r} \frac{\partial}{\partial r} (r v_1) = 0, \quad (9)$$

$$\frac{\partial u_1}{\partial t} + \frac{1}{r} \frac{\partial}{\partial r} [r(u_1 v_0 + u_0 v_1)] + \frac{\partial}{\partial x} (2u_0 u_1) = -\frac{1}{\rho} p'_{x1} + \nu \left[\frac{\partial^2 u_1}{\partial r^2} + \frac{1}{r} \frac{\partial u_1}{\partial r} \right], \quad (10)$$

$$\frac{\partial v_1}{\partial t} + \frac{1}{r} \frac{\partial}{\partial r} (2r v_0 v_1) + \frac{\partial}{\partial x} (u_0 v_1 + u_1 v_0) = -\frac{1}{\rho} p'_{r1} + \nu \left[\frac{\partial^2 v_1}{\partial r^2} + \frac{1}{r} \frac{\partial v_1}{\partial r} - \frac{v_1}{r^2} \right], \quad (11)$$

$$\frac{\partial T_1}{\partial t} + \frac{1}{r} \frac{\partial}{\partial r} [r(v_1 T_0 + T_1 v_0)] + \frac{\partial}{\partial x} (u_0 T_1 + u_1 T_0) = \frac{k}{\rho C_p} \left[\frac{\partial^2 T_1}{\partial r^2} + \frac{1}{r} \frac{\partial T_1}{\partial r} \right]. \quad (12)$$

As usually done, these equations have been reduced by introducing the different dimensionless quantities

$$r^* = r/R, \quad x^* = x/R,$$

$$u^* = u/U, \quad v^* = v/U,$$

$$p_{x^*}^{*'} = \left(\frac{\partial p}{\partial x} \right)^* = (\partial p / \partial x) / (\partial p / \partial x)_p,$$

$$p_{r^*}^{*'} = \left(\frac{\partial p}{\partial r} \right)^* = (\partial p / \partial r) / (\partial p / \partial x)_p,$$

as well as

$$\Omega = \omega R^2 / \nu, \quad \theta^* = (T - T_\infty) / (T_w - T_\infty),$$

$$Re = UR / \nu \quad \text{and} \quad Pe = Re Pr$$

where * will be omitted later, in order to simplify the formulation.

NUMERICAL SCHEME

The resolution method is close to those classical ones given in literature but three main changes are adopted.

1. Equation (2) gives an approximate value for u_i^{j+1} and $p_{x_i}^{j+1}$ by means of a volumetric rate condition, such as

$$\dot{m} = \sum 2\pi r_i \Delta r_i u_i = \text{constant}$$

from an arbitrary value given to the axial pressure gradient.

2. Equation (1) is used here as a refinement for the axial velocity and for the computation of the

radial velocity until a convergence criterion is verified:

$$|(u^{j+1})_n - (u^{j+1})_{n+1}| < \varepsilon = 10^{-3}$$

with n being the iteration order

3. Equation (3) is only used to give the radial pressure gradient for the velocity field, and so could be useless for this convective study.

This new method specifically built to treat this convective problem greatly simplifies the resolution, and consequently reduces the time computation.

For the finite difference resolution, the different functions are calculated with centred steps along the axis and fractional steps along the radius. To describe the progression along the axis a predicting-correcting method has been used. More details are given in Reference 3. As an example the discretized versions of equation (2) for the zeroth (steady) and the first order (unsteady) are given by

$$\begin{aligned} & \frac{1}{r_i \Delta r_i} \left[r_{i+1/2} v_{i+1/2}^j \left(\frac{u_{i+1}^{j+1} + u_i^{j+1}}{2} \right) - r_{i-1/2} v_{i-1/2}^j \frac{u_i^{j+1} + u_{i-1}^{j+1}}{2} \right] + \left(\frac{\ddot{u}_i^{j+1} u_i^{j+1}}{\Delta x_{j+1}} - \frac{u_i^j u_i^j}{\Delta x_{j+1}} \right) \\ & = \frac{8}{Re} p_x^{j+1} + \frac{1}{Re} \left[\frac{1}{\Delta r_i} \left[\frac{u_{i+1}^{j+1} - u_i^{j+1}}{\delta r_{i+1/2}} - \frac{u_i^{j+1} - u_{i-1}^{j+1}}{\delta r_{i-1/2}} \right] + \frac{1}{r_i \Delta r_i} (u_{i+1}^{j+1} - u_{i-1}^{j+1}) \right] \end{aligned} \quad (13)$$

$$\begin{aligned} & u_{1i}^{j+1} \left[j \frac{\Omega}{Re} + \frac{1}{2r_i \Delta r_i} (r_{i+1/2} v_{0i+1/2}^j - r_{i-1/2} v_{0i-1/2}^j) + \frac{u_{0i}^{j+1}}{\Delta x_{j+1}} + \frac{1}{Re \Delta r_i} \left(\frac{1}{\delta r_{i-1/2}} + \frac{1}{\delta r_{i+1/2}} \right) \right] \\ & + u_{1i-1}^{j+1} \left[\frac{-1}{2r_i \Delta r_i} (r_{i-1/2} v_{0i-1/2}^j) - \frac{1}{Re \Delta r_i} \left(\frac{1}{\delta r_{i-1/2}} - \frac{1}{2r_i} \right) \right] \\ & + u_{1i+1}^{j+1} \left[\frac{1}{2r_i \Delta r_i} (r_{i+1/2} v_{0i+1/2}^j) - \frac{1}{Re \Delta r_i} \left(\frac{1}{\delta r_{i+1/2}} + \frac{1}{2r_i} \right) \right] \\ & = - \frac{1}{r_i \Delta r_i} \left\{ r_{i+1/2} \left[v_{1i+1/2}^j \frac{u_{0i+1}^{j+1} + u_{0i}^{j+1}}{2} \right] - r_{i-1/2} \left[v_{1i-1/2}^j \frac{u_{0i}^{j+1} + u_{0i-1}^{j+1}}{2} \right] \right\} \\ & + \frac{8}{Re} p_x^{j+1} + \frac{2}{\Delta x_{j+1}} u_0^j u_{1i}^j \end{aligned} \quad (14)$$

RESULTS

For the zeroth order—steady flow—the dynamic and thermal developing regimes are in good agreement with the results of Langhaar⁴ and Kays.⁵ The small discrepancy between these two models and the present one can be devoted to the radial velocity component, not taken into account in these previous analyses. In a different way, Ulrichson and Schmitz⁶ have deduced the radial velocity from the continuity equation and a linearized axial momentum equation which does not contribute to a real accuracy for the velocity field computation.

For the first order—unsteady flow—Figures 2–4 give the unsteady axial velocity $u_1(r^*, x^*, t)$ versus r^* for different ωt values during the pulsation period; the Reynolds number and the frequency are constant and equal respectively to $Re = 2 \times 10^3$, $\Omega = 100\pi$ for three given x^* values: 22, 40 and 176. These curves confirm the annular effect experimentally described by Richardson and Tyler.⁷ This effect is particularly intense in the entry region (i.e. $x^* = 22$) and decreases progressively with increasing x^* , until the fully steady developed zone, where this effect has disappeared. The maximum for the axial velocity amplitude is located near the wall, and not on the centre

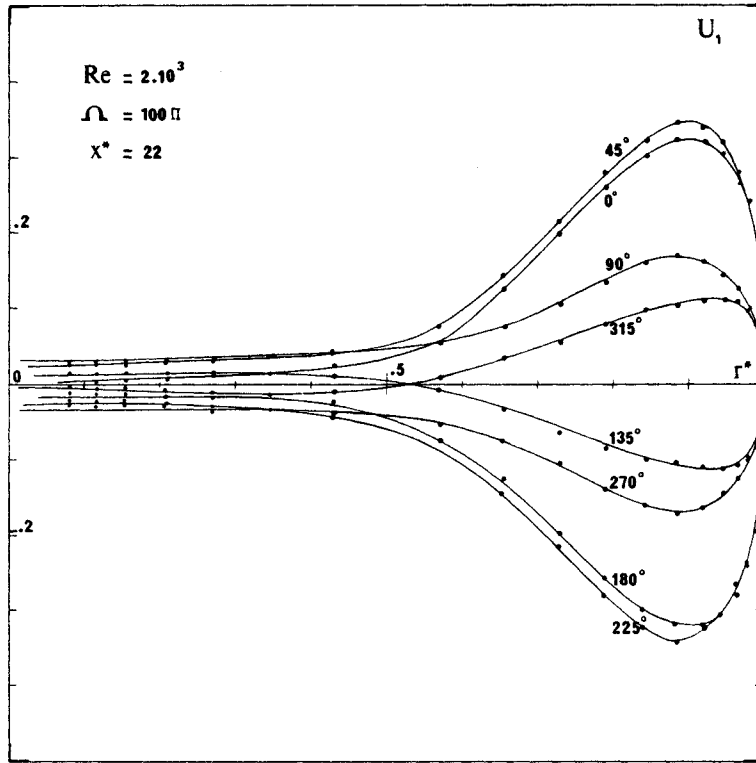


Figure 2. Unsteady axial velocity profiles $x^* = 22$

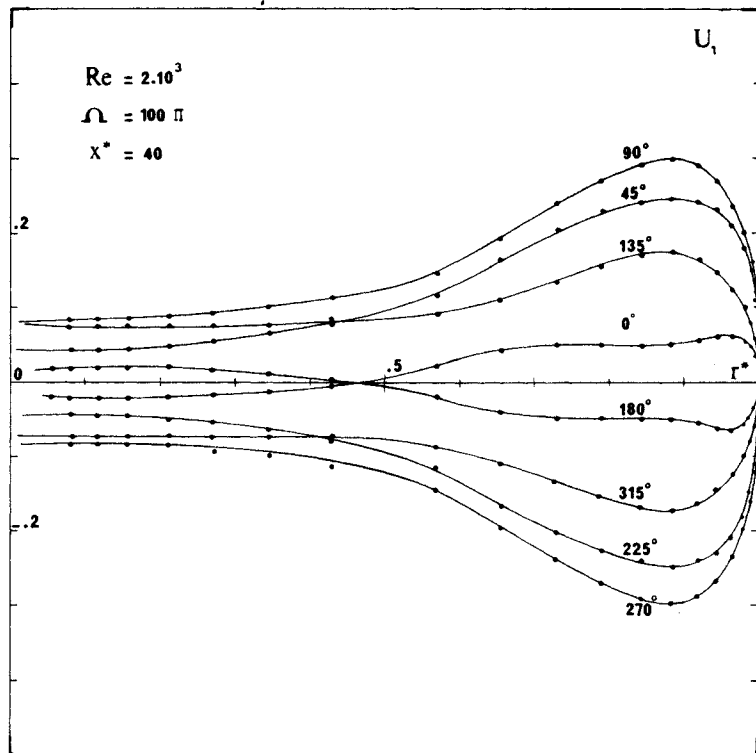


Figure 3. Unsteady axial velocity profiles $x^* = 40$

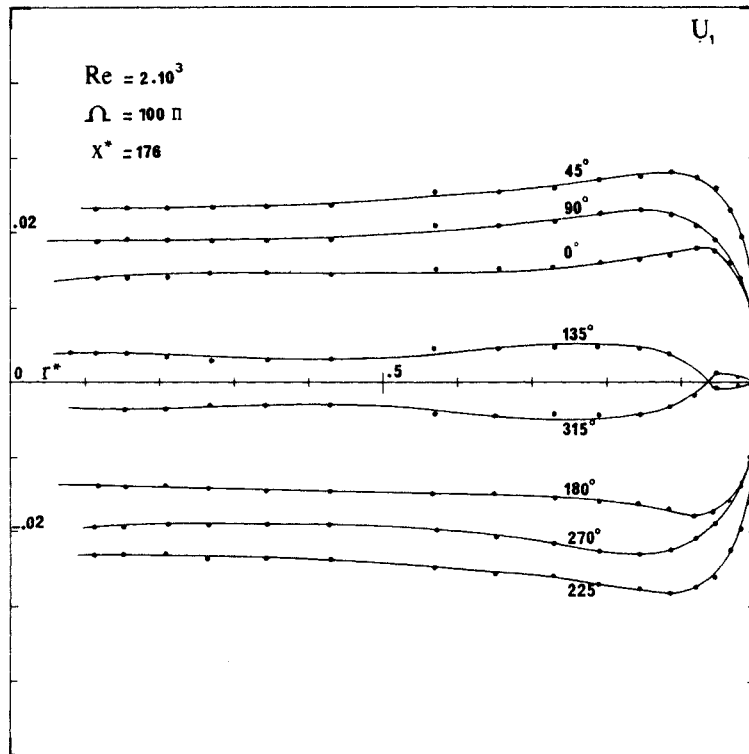
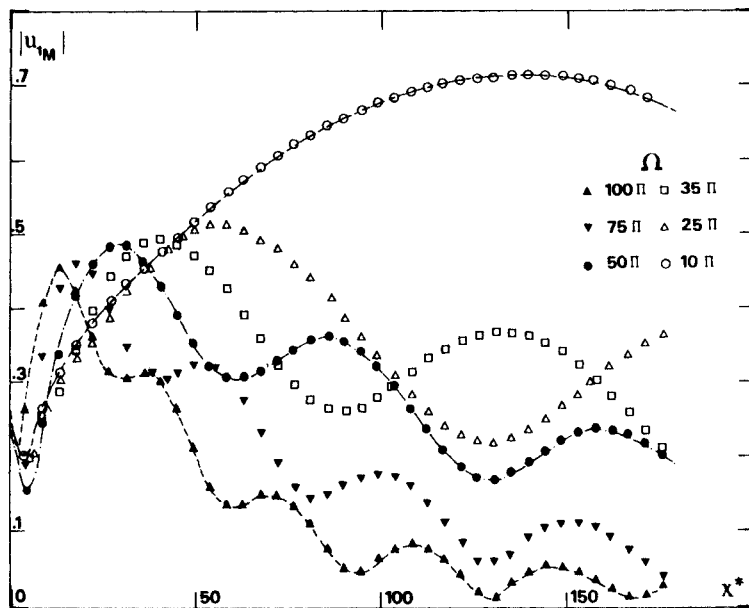
Figure 4. Unsteady axial velocity profiles $x^* = 176$ 

Figure 5. Maximum amplitude evolution for the axial velocity

axis as for the steady flow. It can be noted that the unsteady velocity component in the main core of the flow $0 \leq r \leq 0.5$, is nearly negligible, whereas the effect of the pulsation is mainly located in the region $0.5 \leq r \leq 1$, near the wall.

In Figure 5 the axial evolution for the maximum amplitude u_{1M} versus x^* is shown for different pulsation frequencies. These curves confirm that the maximum amplitude for u_1 decreases when the frequency increases. This last result was already depicted in the fully developed region by Uchida.² However, in the present study concerning the developing zone, the longitudinal evolution for the unsteady axial velocity is not continuously decreasing and can be depicted as a periodical damping phenomenon when progressing inside the tube. The axial length of this periodical damping is inversely proportional to the frequency. The maximum amplitude for u_1 is closer to the tube inlet when the frequency increases. As an example, for a low frequency $\Omega = 10\pi$ the extremum for u_{1M} is located far away from the tube inlet: $x^* = 130$, whereas this extremum for a higher frequency $\Omega = 100\pi$ is near the tube inlet: $x^* = 12$. This induces the following fact: there is a non-negligible annular effect for the unsteady velocity in the developing region, where the fluid is in organization until the fully developed zone. The location of the extremum depends on the frequency.

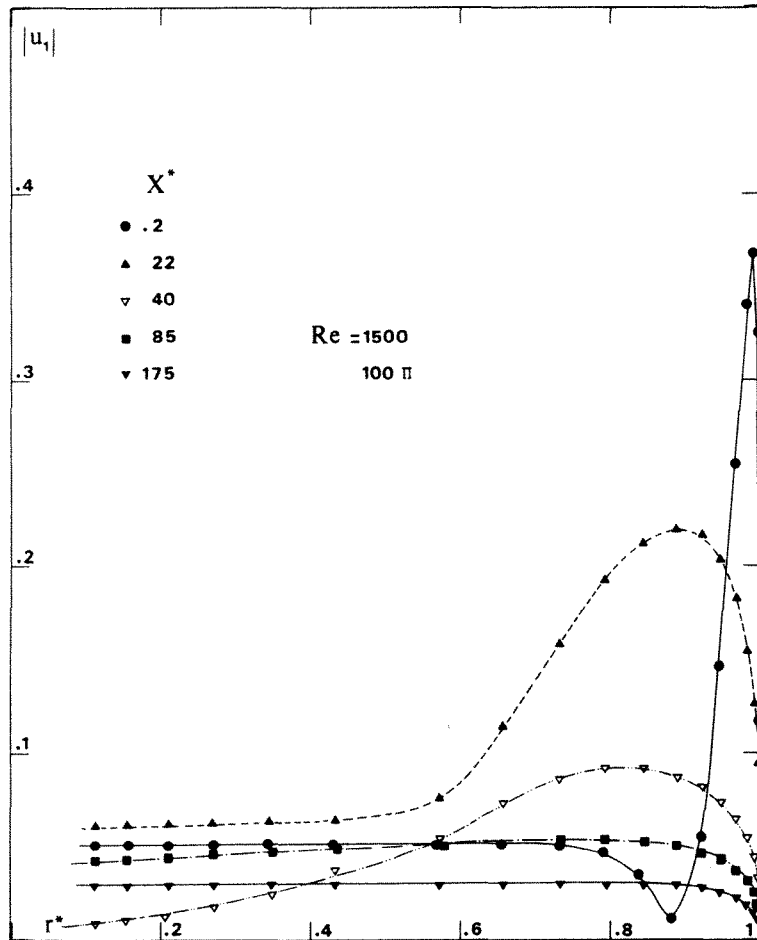


Figure 6. Unsteady velocity modulus $Re = 1.5 \times 10^3$

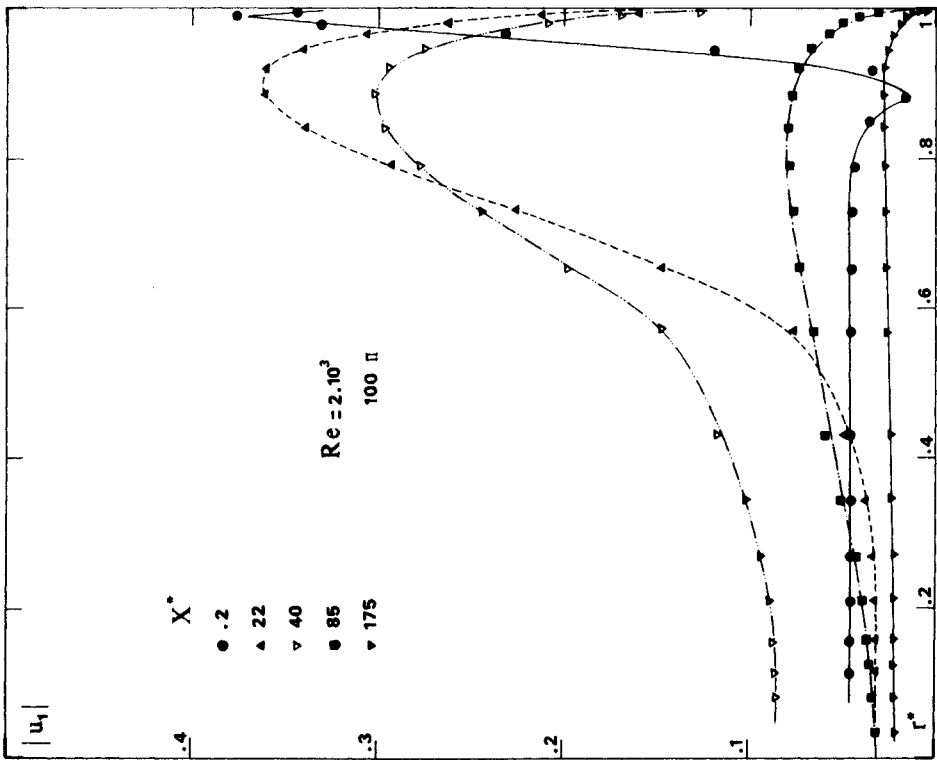


Figure 7. Unsteady velocity modulus $Re = 2 \times 10^3$

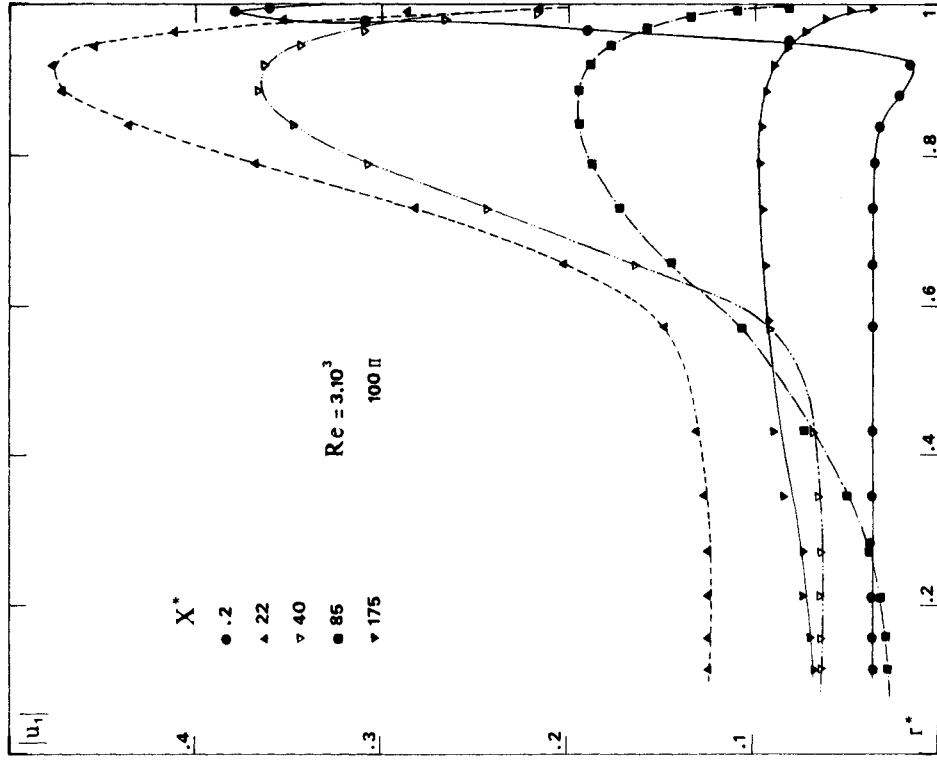


Figure 8. Unsteady velocity modulus $Re = 3 \times 10^3$

To complete the dynamic description Figures 6–8 represent the unsteady velocity modulus versus r^* for the same frequency $\Omega = 100\pi$ and three Reynolds number: $Re = 1500$, $Re = 2000$, $Re = 3000$. As previously stated for the first section, immediately after the entry, $x^* = 0.2$, the different $|u_1|$ values remain constant whatever the Reynolds number is. Beyond the section $x^* = 0.2$ and for the same downstream section, $|u_1|$ increases with the Reynolds number. This effect is more particularly significant for the maximum amplitude of the annular effect. These Figures underline the importance of the unsteady amplitude velocity, and this, more precisely near the entry. The damping of these amplitudes is fast when moving with x^* positive. The modulus ratio for $Re = 2 \times 10^5$, $\Omega = 100\pi$: $|u_1|_{x^*=22}/|u_1|_{x^*=1.75}$ is equal to 31.

This indicates that, near the entry, dynamic fluctuation amplitudes are 31 times greater than these fluctuations amplitudes obtained in the fully developed region. This suggests the existence of an unsteady stress which could lead to a non-negligible effect, when averaged over a period. Significant consequences of such stresses may be expected in the first flow sections (local strains in fluid–structure interactions...). More generally, these effects could be generated not only by a periodic pressure gradient, but also by a *sequential accident* such as a sudden head loss. The particular significance of these unsteady stresses could result from an adequacy of the physical properties, the dynamic parameters of the flow and the unsteady perturbation frequency.

In the same way, the fluid field temperature has been investigated. The unsteady temperature is expressed as follows:

$$\theta_1(x^*, r^*, \Omega, t) = \tau\theta_1(x^*, r^*, \Omega)\cos[\omega t + \psi(x^*, r^*, \Omega)].$$

Figures 9–11 give the unsteady temperature radial profiles for three sections: $x^* = 22$, 40 and

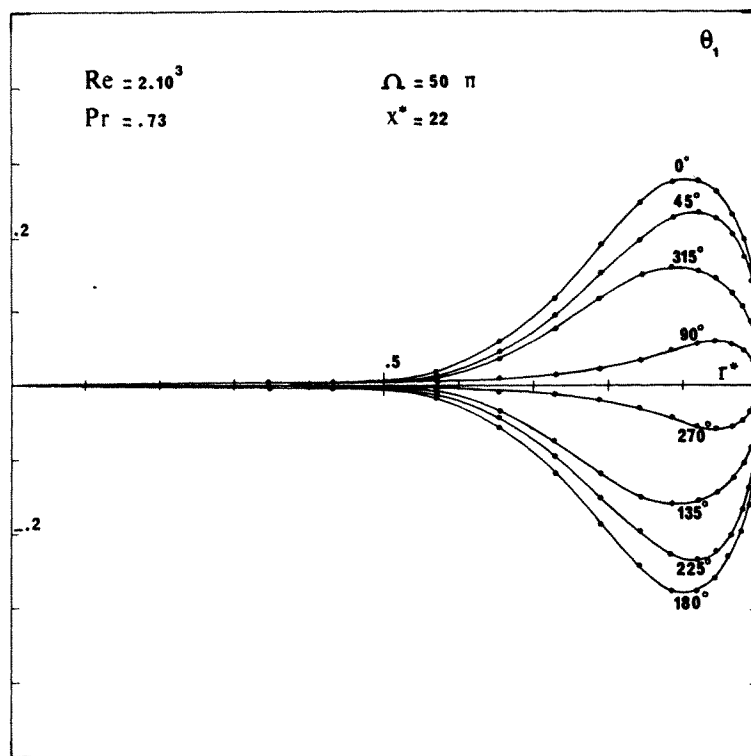


Figure 9. Unsteady temperature profiles $x^* = 22$

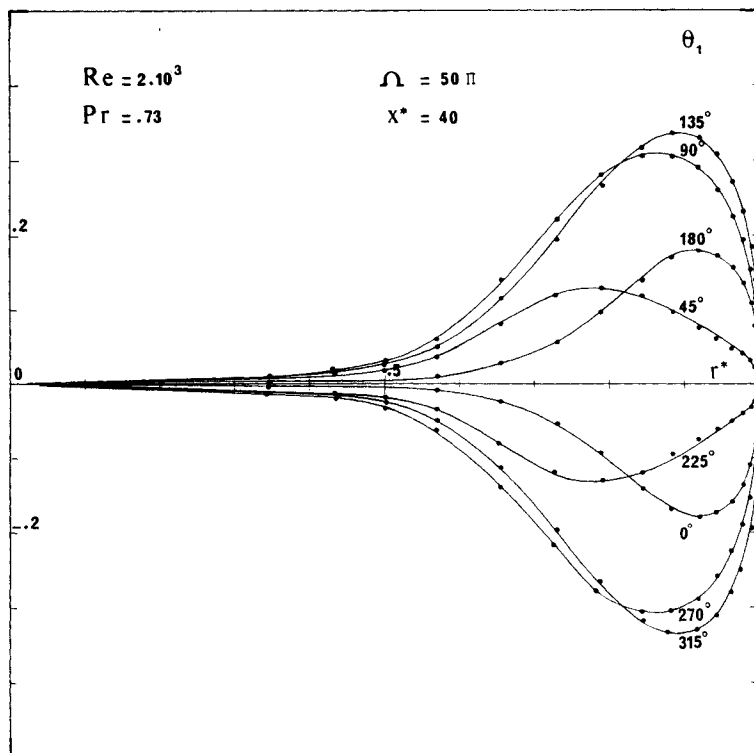


Figure 10. Unsteady temperature profiles $x^* = 40$

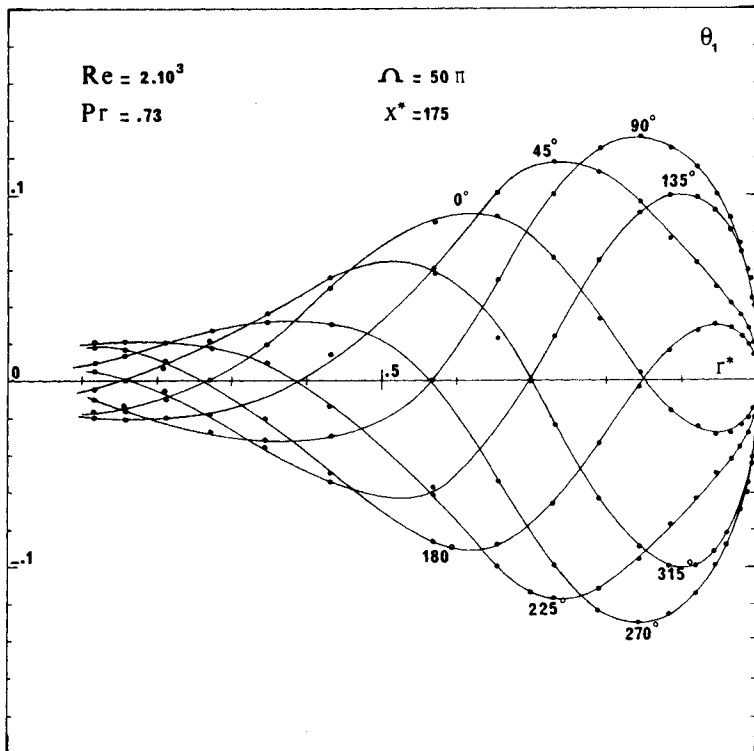


Figure 11. Unsteady temperature profiles $x^* = 176$

176; and $Pr = 0.73$, $Re = 2 \times 10^3$, $\Omega = 50\pi$. From a general point of view, it can be observed that the maximum amplitude does not coincide with the main axis, as it does for the steady temperature profile. This annular effect, not previously depicted, should lead to a new description for heat transfer phenomena between the wall and the fluid. For this chosen frequency (50π) a progressive amplification for the unsteady temperature amplitude exists from the entry section $x^* = 0$, all along the axial co-ordinate, until a maximum is obtained. Thereafter these amplitudes decrease. Simultaneously, when progressing in the tube from $x^* = 0$, the effect of pulsation on the fluid field is not only located in the region $0.5 \leq r \leq 1$ but extends all over the corresponding section: the radial position of the maximum amplitude moves from the neighbourhood of the wall towards the central axis. To obtain a better understanding, the thermal fluid field has been studied by the use of the unsteady temperature modulus. Figures 12–15 represent $|\theta_1(t)|$ versus r^* for $\Omega = 10\pi, 35\pi, 50\pi, 100\pi$; $Pr = 0.73$ and $Re = 2 \times 10^3$.

The previous remarks given on annular effect evolution remain valid. The growth of the unsteady thermal fluid field in each section is increasing from the low frequency case: 10π until 35π , and then decreases when the frequency increases. In other words, it appears that for some given physical conditions of the flow (Pr, Re, \dots) there should exist an optimum in frequency leading to greater thermal unsteady effects in the entry region. Figure 15 reveals the importance of the unsteady temperature modulus near the duct entry by comparison with those obtained in the fully developed region: $|\theta_{1M}|_{x^*=40}/|\theta_{1M}|_{x^*=175}$ is equal to 5.47 for $Re = 2 \times 10^3$, $Pr = 0.73$, $\Omega = 100\pi$. This ratio is equal to 23, for a higher Prandtl number ($Pr = 1.74$) with the same Re

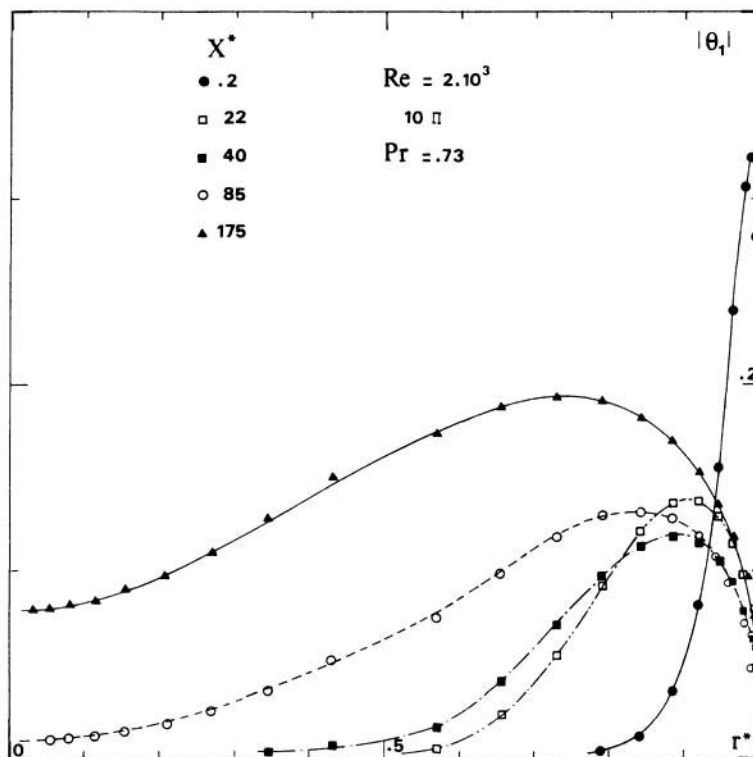


Figure 12. Unsteady temperature modulus $\Omega = 10\pi$

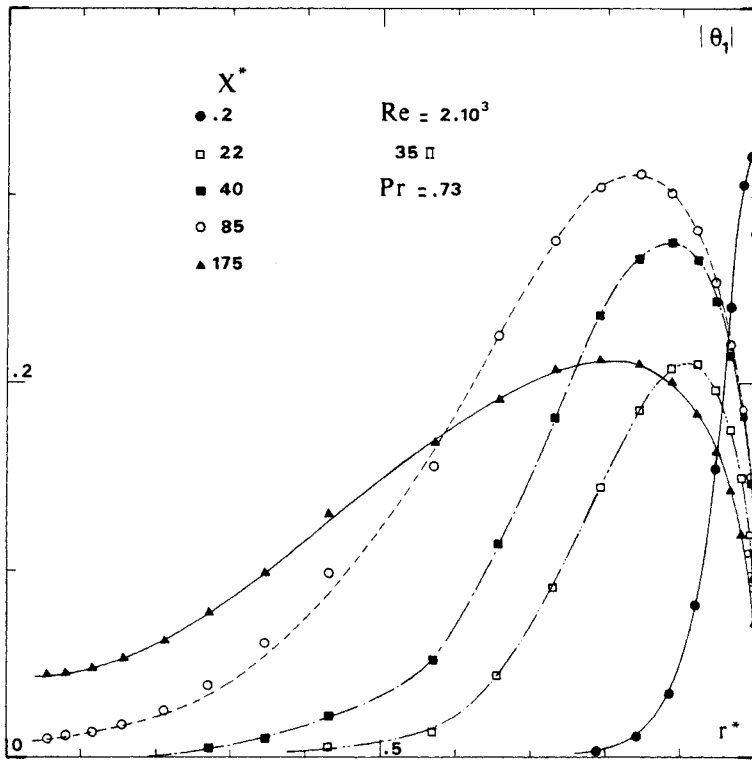


Figure 13. Unsteady temperature modulus $\Omega = 35\pi$

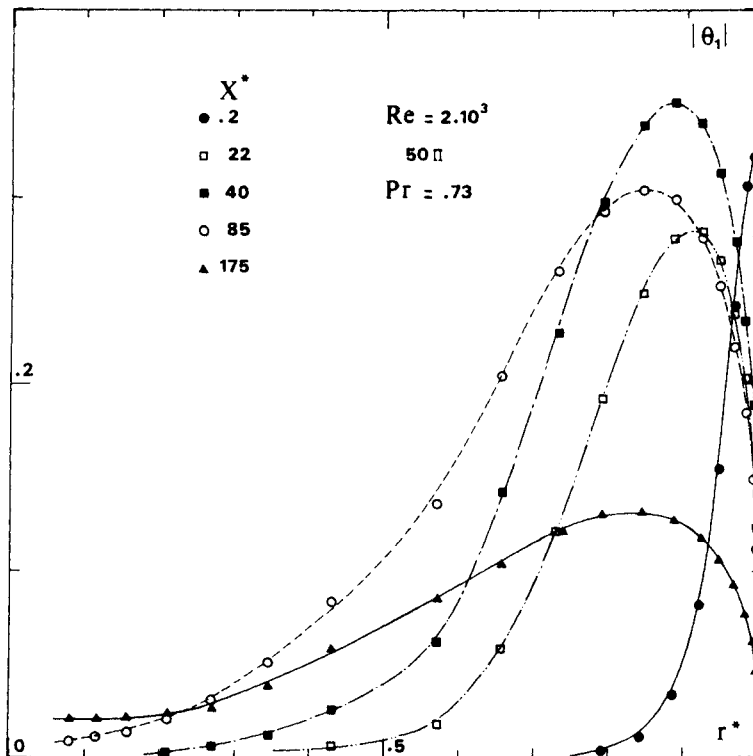


Figure 14. Unsteady temperature modulus $\Omega = 50\pi$

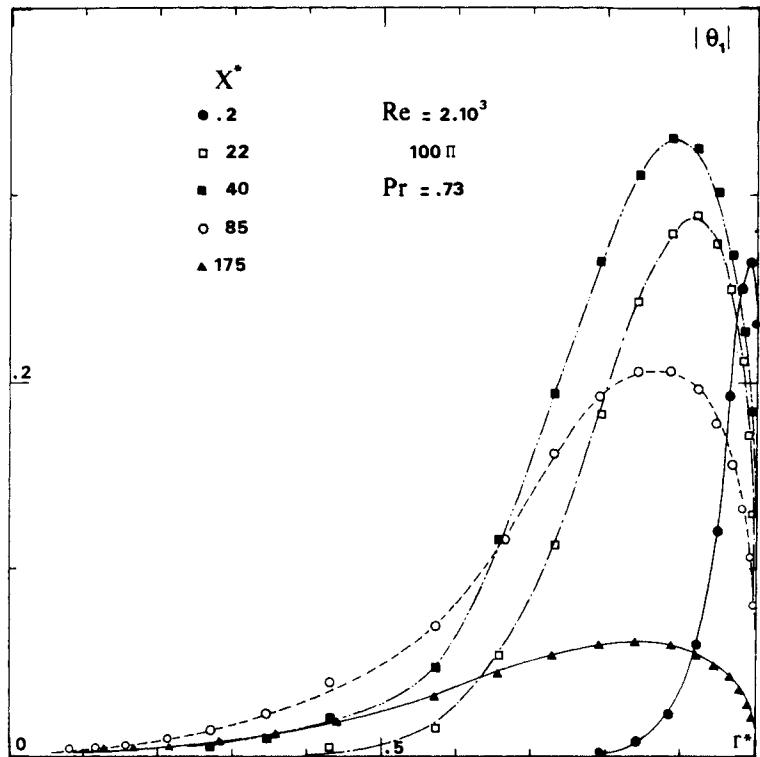


Figure 15. Unsteady temperature modulus $\Omega = 100\pi$

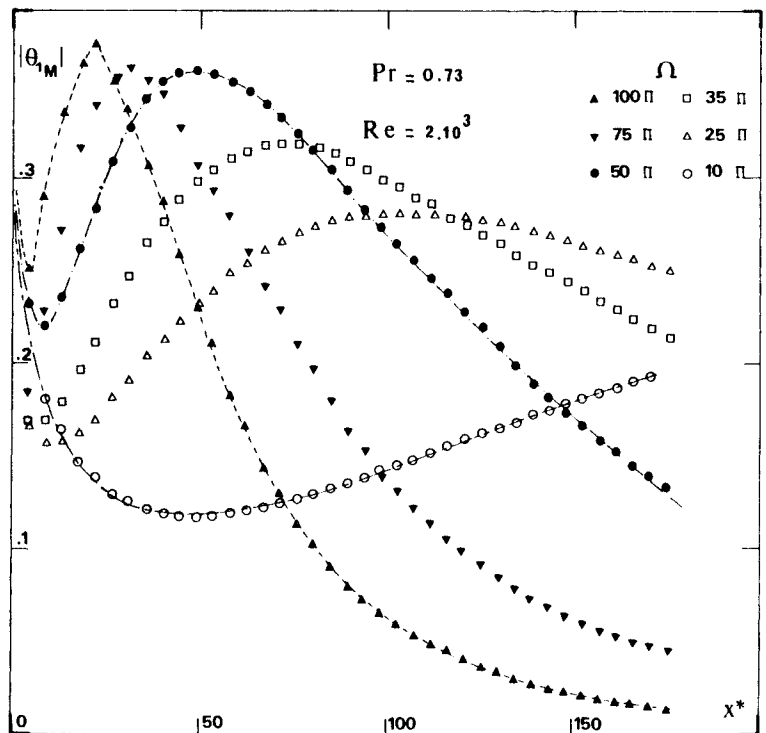


Figure 16. Maximum amplitude evolution for the axial temperature

and Ω conditions. It shows, as for the dynamic study, the existence of a thermal stress in the first steps of the developing flow.

If we try to summarize the previous thermal results by examining the maximum amplitude for $|\theta_1(t)|$ versus the longitudinal co-ordinate, Figure 16 provides a better analysis of the thermal amplitude longitudinal damping. Each curve presents a maximum and a decrease from this maximum. Moreover we can observe if the frequency increases:

- (a) the maximum for $|\theta_{1M}|$ is more important
- (b) this maximum is closer to the entry section
- (c) the damping for $|\theta_{1M}|$ is faster.

It can be noted that there is no periodic damping as previously shown for the unsteady axial velocity.

CONCLUSION

Some results of a numerical model describing the simultaneous dynamic and thermal developments of an unsteady ducted flow are presented. With the assumptions of a laminar regime and an incompressible viscous flow, the influence of a periodic axial pressure gradient is mainly studied in the developing region for different parameter ranges (Reynolds and Prandtl numbers, frequency) and a uniform wall temperature. The results obtained give some precision on those previously shown on the developing steady and fully developed unsteady flows. They particularly show the importance of the entry region for the unsteady dynamic and thermal phenomena and their longitudinal evolutive progression.

Then, the evolution of the annular effect (Richardson effect) for the unsteady axial velocities is expressed for some variations of the two parameters: Reynolds number and frequency. In a general manner, the velocity amplitude maximum, which is located in the vicinity of the wall in the first sections, tends to move progressively towards the centre axis; moreover, this maximum is periodically damped when progressing with the flow. These fluctuations are fast vanishing from the entry to the fully developed zone for higher frequencies.

In this inlet region, unsteady dynamic effects present large amplitudes with respect to those obtained in the fully developed region, i.e. $|u_1|_{x^*=22}/|U_1|_{x^*=175}$ is equal to 31 for $Re = 2 \times 10^3$. These effects are mainly located in the wall region. This suggests the existence of intense unsteady stresses (shear or friction stresses) at the wall. With the model assumptions, these stresses result from a periodic modulation of the axial pressure gradient but could be also generated by a sudden change with time of the upstream flow pressure as, for instance, a sudden head loss. These time-averaged effects could be non-negligible.

Concerning the developing unsteady thermal fluid field, the model points out an annular effect for the temperature profiles with similar properties to those obtained for the corresponding velocity effect. However, the longitudinal damping for the temperature maximum presents no periodicity. As for the dynamic regime, the unsteady thermal fluid field remains mainly located in the wall region for the first sections. Moreover for these first sections, temperature fluctuations have larger amplitudes than in the developed region, i.e. $|\theta_{1M}|_{x^*=22}/|\theta_{1M}|_{x^*=175}$ is equal to 23 for $\Omega = 100$, $Pr = 1.74$ and $Re = 2 \times 10^3$. This leads also to the assumption of unsteady thermal stresses at the wall in this entry region.

The investigated changes for the different parameters (Re , Pr , Ω) show that there could exist an 'adequacy' of them, leading to large amplitudes for the unsteady velocity and temperature in the entry region if compared to those encountered downstream in the fully developed region. This adequacy between the modulation frequency and the dynamic parameters may correspond

to the classical resonance phenomenon. Dynamic and, here, thermal consequences of such a 'pseudo-resonance' could be important in the first flow sections, whereas downstream, inertia and frictional effects lead to a fluctuation damping.

NOMENCLATURE

x	axial co-ordinate
r	radial co-ordinate
t	time
R	tube radius
x^*	x/R ; $x = x/D Re$
r^*	r/R
u	axial velocity component amplitude
v	radial velocity component amplitude
U	mean velocity for the fully developed flow
p	static pressure
u^*	u/U
v^*	v/U
p_x^*	dimensionless axial pressure gradient: $(\partial p/\partial x)^* = (\partial p/\partial x)/(\partial p/\partial x)_p$
p_r^*	dimensionless radial pressure gradient: $(\partial p/\partial r)^* = (\partial p/\partial r)/(\partial p/\partial x)_p$
k	fluid thermal conductivity
C_p	specific heat capacity at constant pressure
Re	Reynolds number (based on radius R)
Pe	Peclet number
Pr	Prandtl number
\dot{m}	mass flow rate
T	local fluid temperature
T_w	wall temperature
T	duct inlet temperature
T_m	mean fluid temperature in a tube section
ρ	mass density
μ	dynamic viscosity
ν	kinematic viscosity
ψ	phase
ω	pulsation
Ω	dimensionless pulsation: $\omega R^2/\nu$
ε	perturbation parameter
τ	modulation rate
θ	$(T - T_\infty)/(T_w - T_\infty)$
0	zeroth order
1	first order

REFERENCES

1. T. SEXTL, 'Über den von E. G. Richardson entdeckten "Annular Effekt"', *Z. für Physik*, **61**, 349–362 (1930).
2. S. UCHIDA, 'The pulsating viscous flow superposed on the steady laminar motion of incompressible fluid in a circular duct', *Z. Angew. Math. Phys.*, **7**, 403–422 (1956).
3. R. CREFF, J. BATINA, P. ANDRE and V. S. KARUNANITHI, 'Numerical model for dynamic and thermal developments of a pulsed laminar ducted flow', *Numerical Heat Transfer*, **6**, 173–188 (1983).

4. H. L. Langhaar, 'Study flow in the transition length of a straight tube', *J. Applied Mechanics, Trans. ASME*, **64**, A. 55-A. 58 (1942).
5. W. M. Kays, 'Numerical solutions for laminar-flow heat transfer in circular tubes', *Trans. ASME*, 1265-1274 (1965).
6. D. L. Ulrichson and R. A. Schmitz, *Int. J. Heat Mass Transfer*, **7**, 253 (1965).
7. E. G. Richardson and E. Tyler, 'The transverse velocity gradient near the mouths of pipes in which an alternating or continuous flow of air is established', *Proc. Roy. Soc.*, **42**, pt. 1, (231), 1-15 (1929).